Velocity field path-planning for single and multiple unmanned aerial vehicles

C. R. McInnes
Department of Aerospace Engineering
University of Glasgow
Glasgow, UK

ABSTRACT

Unmanned aerial vehicles (UAV) have seen a rapid growth in utilisation for reconnaissance, mostly using single UAVs. However, future utilisation of UAVs for applications such as bistatic synthetic aperture radar and stereoscopic imaging, will require the use of multiple UAVs acting cooperatively to achieve mission goals. In addition, to de-skill the operation of UAVs for certain applications will require the migration of path-planning functions from the ground to the UAV. This paper details a computationally efficient algorithm to enable path-planning for single UAVs and to form and re-form UAV formations with active collision avoidance. The algorithm presented extends classical potential field methods used in other domains for the UAV path-planning problem. It is demonstrated that a range of tasks can be executed autonomously, allowing high level tasking of single and multiple UAVs in formation, with the formation commanded as a single entity.

NOMENCLATURE

$\mathbf{A}$	vector potential
C	set of obstacles
$\mathbf{e}$	unit vector
f, F	shaping functions
G	goal point
Q	field strength
R	UAV
S	start point
$\mathbf{u}$	velocity vector
V, $\mathbf{v}$	potential field, velocity vector
W	workspace
$\mathbf{x}$	UAV position vector
Δ	position relative to lead UAV
λ	controller inverse time constant
υ	UAV speed
ψ	UAV heading

1.0 INTRODUCTION

Unmanned aerial vehicles have seen a rapid growth in use for reconnaissance applications with a wide range of vehicle types and capabilities fielded. Most current UAV types require a fixed base-station to up-link way-points to the UAV, which have been determined by a human operator, or possibly by path-planning software hosted by the base-station. As the use of UAVs becomes more commonplace, there is a requirement to de-skill the operation of UAVs to allow untrained operators to use these systems in the field with a minimum of ground equipment. This will require much of the path-planning capability to reside on the UAV with the operator up-linking only high-level goals, which must then be autonomously executed. Such autonomous path-planning must operate in near real-time, must be computationally efficient and must be validated to ensure that the UAV safely achieves its goal.

Future UAV systems will also see the use of multiple UAVs used in formation for tasks such as bistatic synthetic aperture radar and stereoscopic imaging. These systems will require path-planning algorithms which can form and re-form the UAVs while enforcing collision avoidance between members of the formation. In order to plan such reconfigurations as a top-down process is unwieldy for large numbers of UAVs. For example, a group of N UAVs would require $N(N-1)$ constraint checks for collision avoidance in addition to N goal satisfaction checks, so that the problem scales as N^2. However, for a distributed algorithm the problem scales as $N-1$ for each member of the formation. In addition, distributed planning algorithms are inherently more robust and can cope with adding or removing members from the formation without significantly modifying the manner in which the algorithm operates.

The particular scenario envisaged here is for UAVs (possibly micro-air vehicles) using an on-board digital map along with GPS and inertial navigation to manoeuvre in a complex and cluttered environment. The algorithm presented can transform a map of path constraints and goals into a velocity field, with any path through the velocity field guaranteed to be collision-free and to reach the goal. The algorithm is able to generate such paths for a single UAV or for

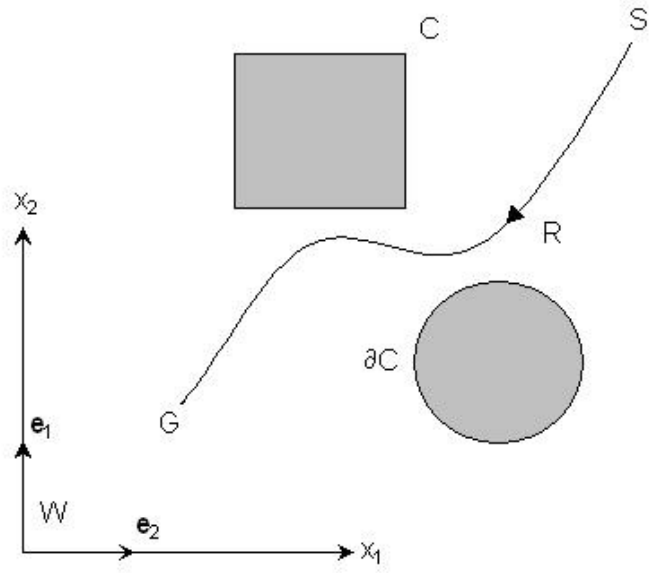

Figure 1. Schematic geometry of the UAV workspace.

multiple UAVs, where each UAV has information on the state of other members of the formation through cross-links. For multiple UAVs, each member of the formation views the other members as mobile obstacles, while the formation configuration is defined through a set of mobile goals towards which each UAV manoeuvres.

Initially a single UAV *R* will be considered moving in a structured workspace $W \in \Re^2$, where the UAV position in *W* is represented by a vector $\mathbf{x} = (x_1, x_2)$, as shown in Fig. 1. The workspace has a set of static obstacles *C*: $x_C = (\tilde{x}_1, \tilde{x}_2)$ with boundary ∂C, a start point *S*: $\mathbf{x}_s = (x_{1s}, x_{2s})$ and a goal point *G*: $\mathbf{x}_G = (x_{1G}, x_{2g})$ towards which *R* manoeuvres. The UAV will be considered to be point-like with bank-to-turn control which can track a heading command, up to some turning rate limit, and a throttle control which can track a speed command. Since *W* is in $\Re^2$ the UAV will manoeuvre at a fixed altitude, although extensions of the method to $\Re^3$ are possible. A path-planning algorithm is now sought which can translate *R* from *S* to *G* without crossing the obstacle boundaries ∂C. An extension of the classical potential field method will be considered here. To broaden the analysis to multiple UAVs in formation, the set of obstacles *C* may also be mobile, with each UAV viewing other UAVs in the formation as an obstacle. In addition, the goal *G* may be also be mobile and may be referenced to the lead UAV in the formation, to enable leader-follower behaviour, or the goal may be referenced to some function of the state of the UAV formation to provide de-centralised control.

The classical application of the potential field method requires an artificial potential function *V* to be superimposed on *W*[1-4]. The potential function is chosen such that it has a single global minimum at *G* and its gradient field $-\nabla V$ directs *R* safely away from *C* towards *G* for any start point $S \in W$. However, for heuristically generated potential functions there may be a set of local minima which can trap *R* in an equilibrium position ($\nabla V = 0$) other than G. To avoid such local minima *V* can be generated as a solution to the Laplace equation ($\nabla^2 V = 0$)[3,4]. The resulting artificial potential function then has the appealing properties of linearity and uniqueness, while its maxima and minima can only occur on the boundaries of the domain. Therefore, the potential is free of local minima and so trapping at positions other than *G* cannot occur. A more 'aggressive' form of path-planning has also been proposed by utilising vortex functions[5-9]. The vortex potential is also a solution to the Laplace equation and is used to generate a solenoidal gradient field which is again free from local minima. Vortex functions also provide a consistent, preferred direction for circumnavigating the obstacle set *C*. However, previous applications of vortex methods have relied on heuristics to blend the gradient and vortex fields. Such heuristic approaches do not lend themselves to rigorous validation.

In this paper vortex functions are extended and used as the basis for a distributed path-planning algorithm for single and multiple UAVs. The first new finding is that the vortex field can be shaped by a scalar function to rapidly truncate its effects beyond the vicinity of the obstacle boundary. The resulting velocity field has zero divergence and so can still in principle satisfy the Laplace equation with its appealing properties. It is also demonstrated that complex, non-symmetric obstacles can also be represented as a solenoidal velocity field, which greatly enhances the use of vortex functions as a path-planning tool. In particular, obstacles can be added to or deleted from the workspace without re-planning the entire UAV path, as would be required by other path-planning algorithms. This is an important capability, which allows the addition of new path planning information as it becomes available. In addition, since the global velocity field can be generated analytically, the on-board computational overhead to implement the algorithm is minimal, allowing autonomous operations with on-board path-planning. While not necessarily fuel or time optimum,[10] the benefits of the potential field method have been recognised for other problem domains[11] and indeed the method has been applied to related air traffic management problems[9,12]. Again, the key advantage for UAV applications is the ability of the method to generate guaranteed collision-free paths in complex workspaces with a minimal computational overhead.

Lastly, it is shown that the vortex velocity field can be derived from a vector potential which can also be extended to represent complex, non-symmetric obstacles by a solenoidal field. Helmholtz's theorem is then invoked to demonstrate that the solenoidal field component represented by the vector potential, used to enforce collision avoidance, can be systematically combined with gradient fields generated from scalar potential functions, used to manoeuvre *R* towards *G*, in a rigorous way. The utility of the algorithm is explored by considering a number of path-planning problems for single and multiple UAVs in formation.

2.0 VORTEX FUNCTIONS

The Laplace equation has been widely used to generate artificial potential functions for mobile robot path-planning either by a numerical grid solution or by utilising a limited class of analytical solutions[3,4]. Solutions to the Laplace equation have the useful property that only a single global minimum will exist at the goal point of the workspace *G*. The Laplace equation is defined by

$$\nabla^2 V(x) = 0 \quad , \quad \nabla^2 = \frac{\partial^2}{\partial x_1^{\,2}}\mathbf{e}_1 + \frac{\partial^2}{\partial x_2^{\,2}}\mathbf{e}_2 \qquad \ldots (1)$$

with two types of analytic solution in $\Re^2$. Type I solutions represent an irrotational source or sink whereas type II solutions represent a solenoidal source. The type I solutions with a sink term can be used to generate a potential which will drive *R* towards *G*, while the type I source and type II functions can be used to direct *R* away from *C* and so enforce collision avoidance using

$$V_I = Q_I \ln\left((x_1 - \tilde{x}_1)^2 + (x_2 - \tilde{x}_2)^2\right) \qquad \ldots (2a)$$

$$V_{II} = Q_{II} \mathrm{Tan}^{-1}\left[\frac{x_2 - \tilde{x}_2}{x_1 - \tilde{x}_1}\right] \qquad \ldots (2b)$$

$$Q_I = \frac{\text{å}}{\text{å} + d} \quad , \quad d = \left((\tilde{x}_1 - x_{1G})^2 + (\tilde{x}_2 - x_{2G})^2\right)^2 \qquad \ldots (2c)$$

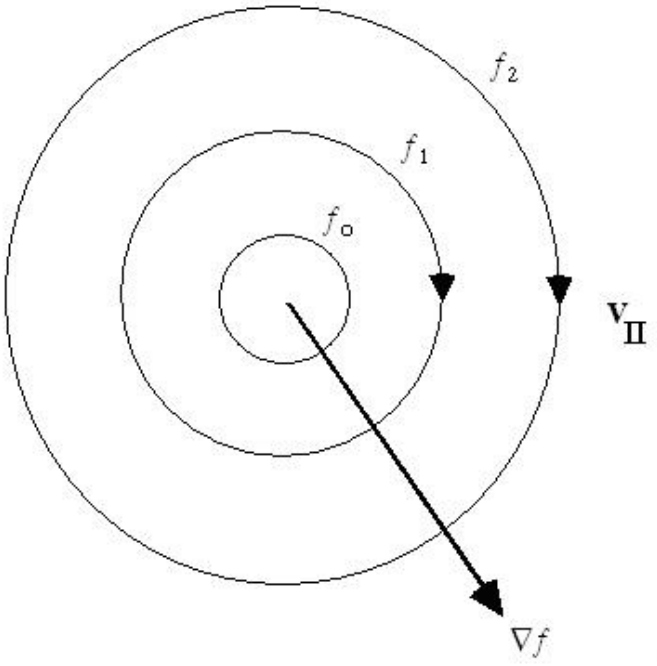

Figure 2(a). Relationship between a symmetric solenoidal field and shaping function f.

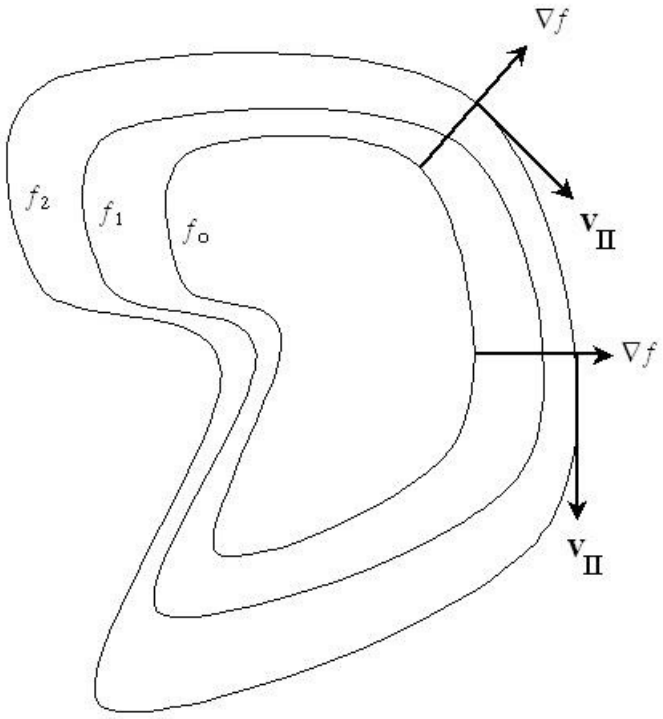

Figure 2(b). Relationship between an asymmetric solenoidal field and shaping function f.

It can be shown that the strength of the type I potential function Q_I may be chosen to satisfy an exclusion zone of radius ε about an obstacle using Equation (2c)[4]. Since the type II potential function is not single-valued there is however no corresponding relationship for the strength Q_{II}. These scalar functions are then used to generate velocity fields through the gradient operator $-\nabla V$ as

$$\mathbf{v}_I = \frac{-(x_1-\tilde{x}_1)Q_I}{\sqrt{(x_1-\tilde{x}_1)^2+(x_2-\tilde{x}_2)^2}}\mathbf{e}_1 - \frac{(x_2-\tilde{x}_2)Q_I}{\sqrt{(x_1-\tilde{x}_1)^2+(x_2-\tilde{x}_2)^2}}\mathbf{e}_2 \quad \text{. . (3a)}$$

$$\mathbf{v}_{II} = \frac{(x_2-\tilde{x}_2)\mathrm{Q}_{\mathrm{II}}}{(x_1-\tilde{x}_1)^2+(x_2-\tilde{x}_2)^2}\mathbf{e}_1 - \frac{(x_1-\tilde{x}_1)\mathrm{Q}_{\mathrm{II}}}{(x_1-\tilde{x}_1)^2+(x_2-\tilde{x}_2)^2}\mathbf{e}_2 \quad \text{. . (3b)}$$

where it can be shown that both velocity fields have null divergence

$$\nabla.\mathbf{v}_I = 0 \;\Rightarrow\; \nabla^2 V_I = 0 \quad \text{. . (3c)}$$

$$\nabla.\mathbf{v}_{II} = 0 \;\Rightarrow\; \nabla^2 V_{II} = 0 \quad \text{. . (3d)}$$

since they are both generated from solutions to the Laplace equation.

Although there is no relationship for the strength Q_{II}, it will now be shown that it is possible to truncate the type II velocity field by a scalar shaping function f while ensuring that the resulting new velocity field still has null divergence. Therefore, if we postulate that the new velocity field is derived from the gradient of some potential, this potential will satisfy the Laplace equation. Since only the gradient of the field is to be used, the potential can however remain unknown. A new velocity field $f\mathbf{v}_{II}$ will therefore be considered with f chosen such that the field has null divergence so that

$$\nabla.(f\,\mathbf{v}_{II}) = \nabla f.\mathbf{v}_{II} + f(\nabla.\mathbf{v}_{II}) = 0 \quad \text{. . (4)}$$

Therefore, since $\nabla.\mathbf{v}_{11} = 0$ the following property is required of the shaping function f

$$\nabla f.\mathbf{v}_{II} = 0 \;\Rightarrow\; f = f(\hat{\imath}) \;,\; \hat{\imath} = \left((x_1-\tilde{x}_1)^2+(x_2-\tilde{x}_2)^2\right)^2 \quad \text{. . (5)}$$

It is clear then that ∇f and $\mathbf{v}_{II}$ must be normal, as shown Fig. 2(a). Since $\mathbf{v}_{II}$ is solenoidal, f must therefore be a function of the radial distance ξ from the centre of the vortex. However, in addition to such azimuthally symmetric functions, it is also possible to generate solenoidal fields for more complex objects through a particular construction of the velocity field $\mathbf{v}_{II}$. In particular, if $\mathbf{v}_{II}$ is defined as

$$\mathbf{v}_{II} = -\frac{\partial f}{\partial x_2}\mathbf{e}_1 + \frac{\partial f}{\partial x_1}\mathbf{e}_2 \quad \text{where} \quad \nabla f = \frac{\partial f}{\partial x_1}\mathbf{e}_1 + \frac{\partial f}{\partial x_2}\mathbf{e}_2 \quad \text{. . (6)}$$

then it is clear that the condition $\nabla f.\mathbf{v}_{II} = 0$ is always satisfied for any smooth scalar function f, as shown in Fig. 2(b). Therefore, by a suitable choice of function f, the magnitude of individual symmetric vortex functions $f\mathbf{v}_{II}$ can be rapidly truncated so that vortices may be superimposed without overlapping influence. Or indeed, more complex solenoidal fields can be generated through a suitable choice of f and the construction of the velocity field using Equation (6). Truncating the effect of the vortex velocity field in a smooth, continuous manner will also allow complex velocity fields to be generated without discrete switching of components of the velocity field as obstacles are approached. Such discrete switching leads to complex hybrid control problems where stability is difficult to ensure. The resulting global velocity field generated here however will be smooth and will have null divergence, so in principle retaining the properties of the Laplace equation, as discussed above.

In order to use any of the velocity fields discussed above, a field strength or shaping function f must be determined which rapidly truncates the effect of the field and ensures that R does not cross the boundary ∂C of the obstacle set C. For a type I irrotational field, such as that defined by Equation (2a), the field strength Q_I may be chosen to satisfy an exclusion zone about an obstacle, as defined by Equation 2(c). An example of the resulting velocity field is shown in

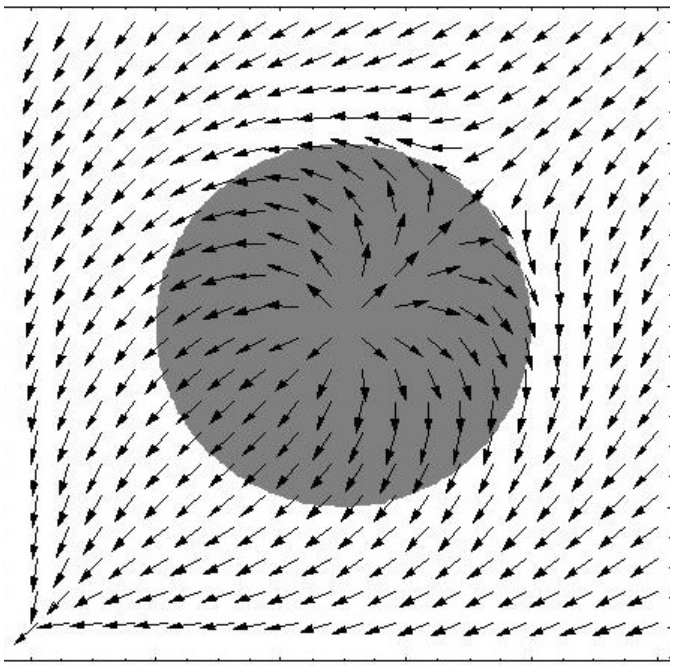

Figure 3(a). Velocity field generated by an irrotational type I potential.

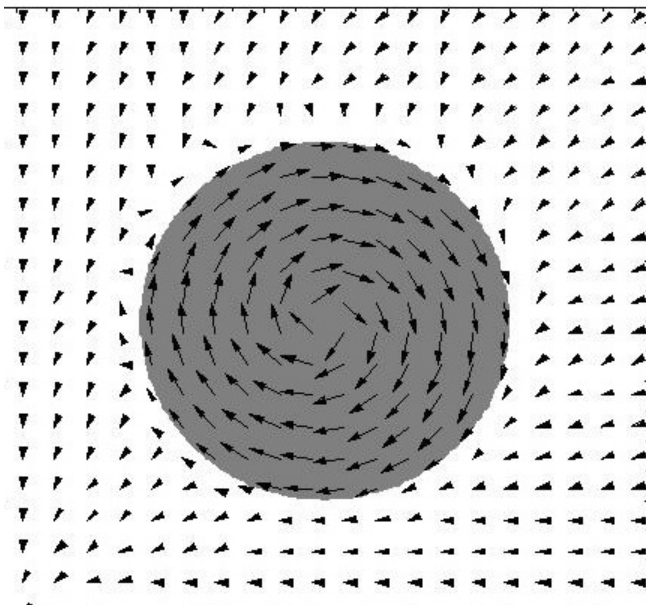

Figure 3(b). Velocity field generated by a solenoidal type II potential.

Fig. 3(a). For a symmetric vortex field, the velocity field itself must be shaped to form $f\mathbf{v}_{II}$. A suitable function for shaping a symmetric vortex field is found to be

$$f = \frac{1}{1+\left(\tilde{\imath}/\hat{\imath}\right)^m} \quad , \quad \hat{\imath} = \left(\left(x_1-\tilde{x}_1\right)^2+\left(x_2-\tilde{x}_2\right)^2\right)^2 \qquad . . (7)$$

where $\tilde{\xi}$ is the radius of influence of the vortex field, which is chosen to enclose the obstacle. If $m >> 1$ then f switches in a rapid, but continuous manner from 1 to 0 as the radius of influence of the vortex field is crossed, as shown in Fig. 3(b). For a more complex obstacle, the obstacle boundary ∂C may be mapped by f and a solenoidal velocity field generated using the construction of Equation (6). For example, a superquadratic function[13] may be used to map a square obstacle using

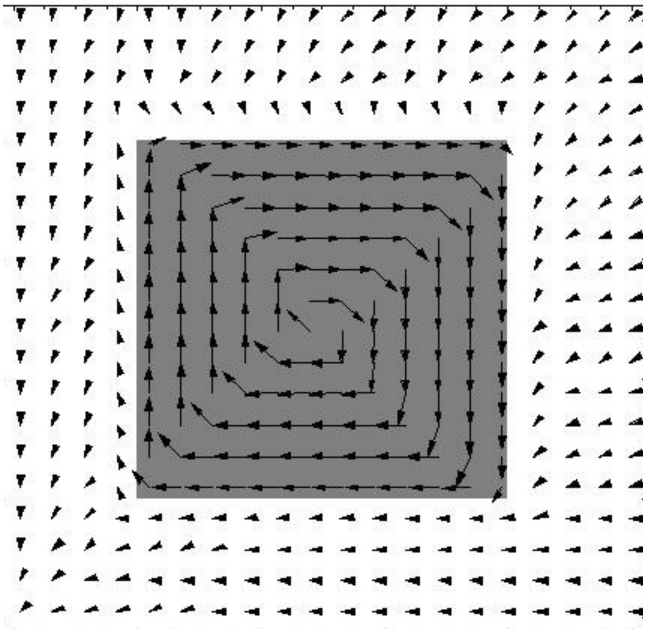

Figure 3(c). Velocity field resulting from a superquadratic generating function.

$$f = H^{-1} \quad , \quad H = \left(x_1-\tilde{x}_1\right)^n+\left(x_2-\tilde{x}_2\right)^n \qquad . . (8)$$

where $n >> 1$ to ensure a sharp edge to the obstacle boundary ∂C. Using Equation (6), and Equation (8) as a generating function, the resulting solenoidal velocity field is found to be

$$\mathbf{v}_{II} = \frac{n\left(x_2-\tilde{x}_2\right)^{n-1}}{\left(\left(x_1-\tilde{x}_1\right)^n+\left(x_2-\tilde{x}_2\right)^n\right)^2}\mathbf{e}_1 - \frac{n\left(x_1-\tilde{x}_1\right)^{n-1}}{\left(\left(x_1-\tilde{x}_1\right)^n+\left(x_2-\tilde{x}_2\right)^n\right)^2}\mathbf{e}_2 \qquad . . (9)$$

While the shaped velocity field $f\mathbf{v}_{II}$ has null divergence, as discussed earlier, it also possible to shape the velocity field defined by Equation (9) in a different manner to form a new velocity field $F(H)\mathbf{v}_{II}$, where the function F is a function of H only. With this construction it can be shown that $\nabla.(F\mathbf{v}_{II}) = 0$ since

$$\nabla.\left(F\,\mathbf{v}_{II}\right) = \nabla F.\mathbf{v}_{II} + F\left(\nabla.\mathbf{v}_{II}\right) = 0 \qquad . . (10)$$

where again $\nabla.\mathbf{v}_{II} = 0$ by definition. Then, using Equations (6) and (8) it can be seen that

$$\nabla F.\mathbf{v}_{II} = -\frac{\mathrm{d}F}{\mathrm{d}H}\frac{\partial H}{\partial x_1}\left(-\frac{1}{H^2}\right)\frac{\partial H}{\partial x_2} + \frac{\mathrm{d}F}{\mathrm{d}H}\frac{\partial H}{\partial x_2}\left(-\frac{1}{H^2}\right)\frac{\partial H}{\partial x_1} = 0 \qquad . . (11)$$

A suitable function for shaping the superquadratic solenoidal field is found to be

$$F = \frac{1}{1+\left(\frac{1}{L}H^{\frac{1}{n}}\right)^m} \qquad . . (12)$$

where L is the length scale of the superquadratic, which is chosen to enclose the obstacle. Again, if $m >> 1$ then F switches in a rapid, but continuous manner from 1 to 0 as the edge of the superquadratic side is crossed, as shown in Fig. 3(c).

3.0 VECTOR POTENTIALS

The vector potential is used extensively in electromagnetic theory to represent currents which generate solenoidal magnetic fields[14]. As such it also offers a systematic and rigorous means of generating solenoidal fields for path-planning problems. For a vector potential **A** the resulting velocity field will be defined as

$$\mathbf{v}_{II} = \nabla \times \mathbf{A} \qquad \ldots (13)$$

where the vector potential is obtained by integration from the Biot-Savart law[14]. It can be seen from Equation (13) that the vector potential is not uniquely defined. Any quantity with zero vector curl can be added to the potential without affecting the resulting velocity field.

To illustrate the method, the symmetric shaped vortex function discussed in Section 2 will now be considered with a vector potential defined by

$$\mathbf{A} = \ddot{o}\, \mathbf{e}_3 \quad , \quad \mathbf{e}_3 = \mathbf{e}_1 \times \mathbf{e}_2 \qquad \ldots (14)$$

where, using the Biot-Savart law[14], it is found that

$$\phi = \int \frac{f(\hat{\imath})}{\hat{\imath}} \mathrm{d}\xi + K \quad , \quad \hat{\imath} = \left((x_1 - \tilde{x}_1)^2 + (x_2 - \tilde{x}_2)^2 \right)^{1/2} \qquad \ldots (15)$$

where K is an arbitrary constant of integration. The resulting velocity field is then obtained from Equation (13) as

$$\nabla \times \mathbf{A} = \frac{(x_2 - \tilde{x}_2)\ddot{o}'}{\sqrt{(x_1 - \tilde{x}_1)^2 + (x_2 - \tilde{x}_2)^2}} \mathbf{e}_1 - \frac{(x_1 - \tilde{x}_1)\ddot{o}'}{\sqrt{(x_1 - \tilde{x}_1)^2 + (x_2 - \tilde{x}_2)^2}} \mathbf{e}_2 \qquad \ldots (16)$$

where $\phi' = f(\xi)/\xi$ so that the shaped vortex velocity field is recovered as expected such that

$$\nabla \times \mathbf{A} = f \mathbf{v}_{II} \qquad \ldots (17)$$

From Equation (15) it is clear that only the shaping function f is required to generate the vector potential and so the resulting solenoidal field. Therefore, for complex obstacles a solenoidal field may be generated by using a more complex scalar function, such as a superquadratic, to represent the shape of the obstacle, as discussed in Section 2. The vector potential then gives a rigorous and systematic means of generating a solenoidal velocity field from a scalar function. In addition, the vector potential may now be used with Helmholtz's theorem (a detailed proof of which is given elsewhere[15]) to generate global velocity fields.

Theorem: A vector field with both source and circulation densities vanishing at infinity may be written as the sum of two parts, one of which is irrotational the other solenoidal[15].

Helmholtz's theorem therefore allows a composite velocity field with an attractive goal potential centred on G and solenoidal vector potentials to represent the set of obstacles C to be written as

$$\mathbf{v} = -\nabla V_I + \sum \nabla \times \mathbf{A} \qquad \ldots (18)$$

The properties of the vector field defined by Equation (18) can be investigated by calculating the divergence of the field as

$$\nabla . \mathbf{v} = -\nabla^2 V_I + \sum \nabla . (\nabla \times \mathbf{A}) \qquad \ldots (19)$$

Clearly the first term of Equation (19) will vanish since the potential V_I satisfies the Laplace equation. However, it is a vector property that the divergence of any solenoidal field vanishes so that

$$\nabla . (\nabla \times \mathbf{A}) = 0 \qquad \ldots (20)$$

Therefore, it has been shown that $\nabla . \mathbf{v} = 0$ so that the global field has null divergence. If we again postulate that the field can, in principle, be derived as the gradient of a scalar potential, then the potential will satisfy the Laplace equation and so will be free of local minima. Again, since only the gradient is being used, the form of the actual potential can remain unknown. The gradient field will therefore have a unique goal point G, which will be reached by R from any start point $S \in W$ without trapping or collision with the obstacle set C. We now have a rigorous and systematic means of generating velocity fields which can be used to provide path-planning for negotiating complex obstacles.

Lastly, it is clear from Figs 3(b) and 3(c) that for a rapidly truncating function f the resulting behaviour of R as it manoeuvres from S to G is similar to edge following. Edge following is a simple and effective means of sensory based navigation used by mobile robots for negotiating obstacles in a closed workspace. For a set of obstacles in a workspace, topology ensures that edge following guarantees negotiation of the obstacles. This can be seen from the strong analogy with escape from a maze — with one hand in contact with a wall of the maze, the maze topology guarantees that an exit will always be reached. Similarly, the solenoidal fields generated about obstacles provide a consistent direction for negotiation along the edges of those obstacles with resulting motions about C and towards G from any point S. Therefore, the ability of edge following to provide an effective means of obstacle negotiation without trapping can be seen as equivalent to the property of the solenoidal vector field and the Laplace equation that no local minima are generated.

4.0 VELOCITY FIELD TRACKING

The velocity field to be used to command the UAV will be generated by normalising **v** to provide a unit vector field. This unit vector field provides a unique heading command, with the UAV speed being controlled independently, as will be discussed below. The desired UAV velocity vector $\mathbf{u} = (u_1, u_2)$ will now be defined as

$$\mathbf{u} = \hat{e}(x_1, x_2) \frac{\mathbf{v}}{\|\mathbf{v}\|} \qquad \ldots (21)$$

where the function κ is a scalar function used to control the UAV speed. In particular, κ can defined to be inversely proportional to the curvature of the path to allow tracking of the desired velocity field without actuator saturation through turning rate limits. In order to generate commands for the UAV, the required velocity **u** will be resolved into a scalar speed command υ_c and heading command ψ_c as

$$\tilde{o}_c = \hat{e}(x_1, x_2) \qquad \ldots (22a)$$

$$\mathrm{Tan}\phi_c = \frac{u_2}{u_1} \qquad \ldots (22b)$$

Since the detailed responses of the UAV will not be considered here, these commands are assumed to be effected through a simple first order control with saturation, such that

$$\dot{\tilde{o}} = -\ddot{e}_{\tilde{o}} (\tilde{o} - \tilde{o}_c) \text{ if } |\dot{\tilde{o}}| \le \dot{\tilde{o}}_{\max} \qquad \ldots (23a)$$

$$\dot{\phi} = -\ddot{e}_{\phi} (\phi - \phi_c) \text{ if } |\dot{\phi}| \le \dot{\phi}_{\max} \qquad \ldots (23b)$$

where the constants λ_υ and λ_ψ are the inverse time constants of the UAV response to commanded changes in speed and heading. The motion of the UAV will then be propagated through the velocity field using Equations (22) and (23) and by integrating the kinematic relations

$$\dot{x}_1 = \tilde{o}\mathrm{Cos}\phi \qquad \ldots (24a)$$

$$\dot{x}_2 = \tilde{o}\mathrm{Sin}\phi \qquad \ldots (24b)$$

In order to provide a realistic response, the maximum UAV turn rate $\dot{\psi}_{\max}$ is defined as $10° s^{-1}$ and the maximum acceleration $\dot{\upsilon}_{\max}$ defined as 0·1 g. The time constants are defined as $\lambda_\psi^{-1} = 1s$ for the heading controller and $\lambda_\upsilon^{-1} = 10s$ for the speed controller.

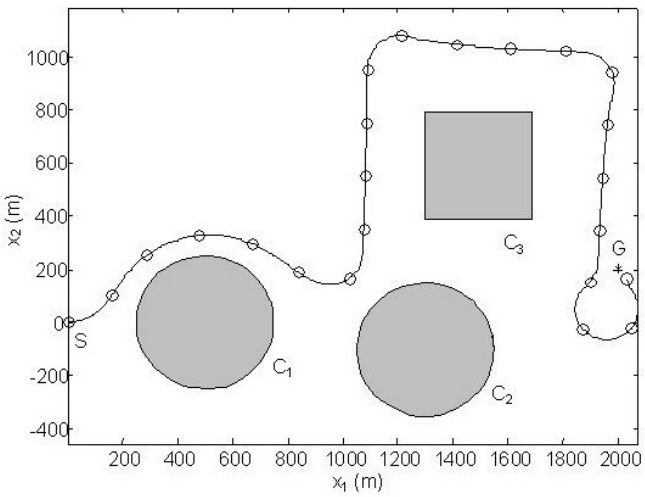

Figure 4(a). Single UAV manoeuvering from a start point S to a goal point G with a set C of three obstacles (o - 10 s time steps).

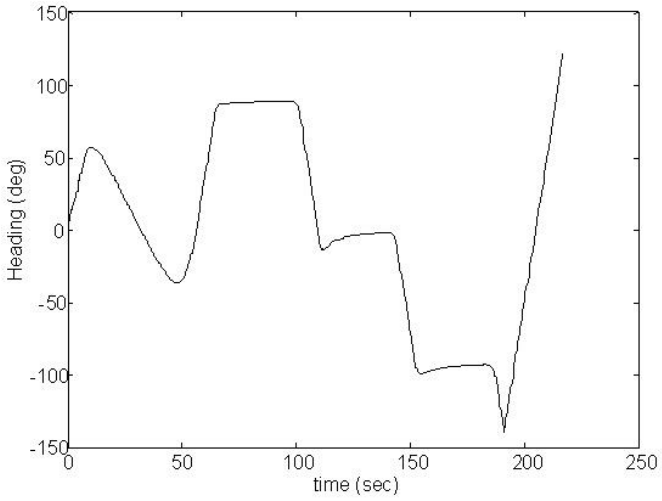

Figure 4(b). UAV heading time history.

5.0 IMPLEMENTATION

In order to illustrate the use of the solenoidal vector fields generated in Sections 2 and 3, a single UAV will be considered manoeuvring from *S* to *G* without crossing the boundary ∂C of a set of static obstacles *C*. The UAV uses the first order controller, time constants and saturation limits defined in Section 4. A set of three obstacles will be defined using the type II velocity field, with two symmetric vortices and a superquadratic generating function used to ensure that the boundaries of the obstacles are not crossed, as shown in Fig. 4(a). Here, the size of the obstacles have been extended by the turning radius of the UAV ($\dot{\upsilon}_{max}/\dot{\psi}_{max}$) to ensure collision avoidance in the presence of controller saturation. In addition, the goal G is represented through a type I velocity field

$$\mathbf{v}_G = \frac{-(x_1 - x_{1G})}{\sqrt{(x_1 - x_{1G})^2 + (x_2 - x_{2G})^2}}\mathbf{e}_1 - \frac{(x_2 - x_{2G})}{\sqrt{(x_1 - x_{1G})^2 + (x_2 - x_{2G})^2}}\mathbf{e}_2 \quad \ldots (25)$$

It can be seen that the UAV successfully negotiates the obstacles and reaches the goal *G* without collision. Since a lag is introduced in heading changes, the UAV does not pass exactly through G. At the end point of the path the UAV passes the goal and executes a left turn to pass the goal again. Subsequent passes are made as the velocity field forces the AUV to loiter in the vicinity of the goal. In this example the UAV speed has been fixed at 20ms^{-1} so that the only active control is the UAV heading, as shown in Fig. 4(b). It can be seen that a series of turns are commanded by the algorithm to avoid the set of obstacles, with a final left turn towards the goal.

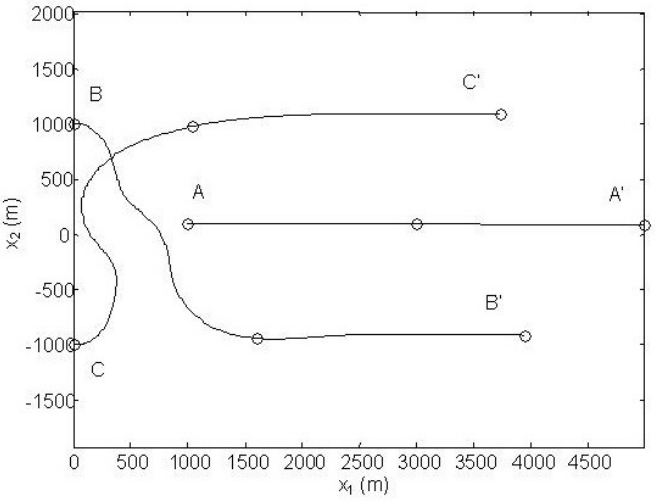

Figure 5(a). Re-formation of a group of three UAVs (o – 100s time steps).

6.0 EXTENSION TO UAV FORMATIONS

The algorithm will now be extended to a group of *N* UAVs flying in formation. The UAV formation-flying problem has been investigated previously, although emphasis has been on maintaining formations[16,17] rather than re-configuration with collision avoidance between members of the formation. Those methods which do consider re-configuration and rely on centralised planners are found to be computationally intensive[18].

The extension of the velocity field algorithm to UAV formations can be achieved using a range of schemes. However, the simplest scheme to implement is for each UAV to treat the remaining *N*–1 UAVs as a set of mobile obstacles *C* and to reference the goal G for each UAV to a designated lead UAV. If the lead UAV has some instantaneous position $\mathbf{x}_L = (x_{1L}, x_{2L})$ and the formation is defined such that the *i*th UAV has a position $(\Delta_i = (\Delta_{1i}, \Delta_{2i})(i = 1 - (N–1))$ relative to the lead UAV, the goal velocity field for the *i*th UAV is defined by a type I velocity field of the form

$$\mathbf{v}_{iG} = \frac{-(x_{1i} - (x_{1L} + \Delta_{1i}))}{\sqrt{(x_{1i} - (x_{1L} + \Delta_{1i}))^2 + (x_{2i} - (x_{2L} + \Delta_{2i}))^2}}\mathbf{e}_1 - \frac{(x_{2i} - (x_{2L} + \Delta_{2i}))}{\sqrt{(x_{1i} - (x_{1L} + \Delta_{1i}))^2 + (x_{2i} - (x_{2L} + \Delta_{2i}))^2}}\mathbf{e}_2 \quad \ldots (26)$$

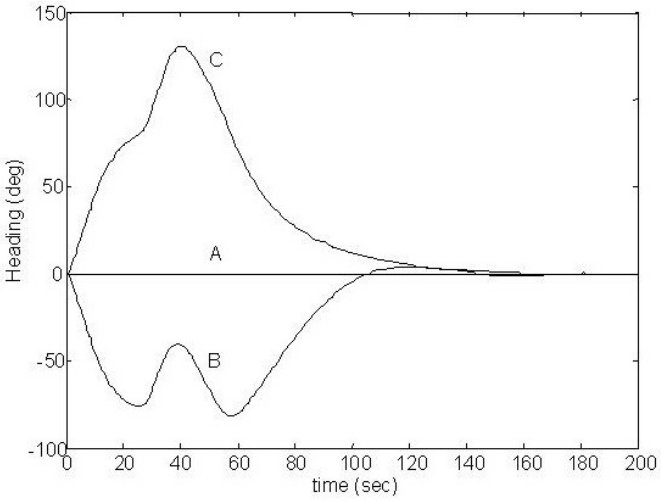

Figure 5(b). UAV formation heading time history.

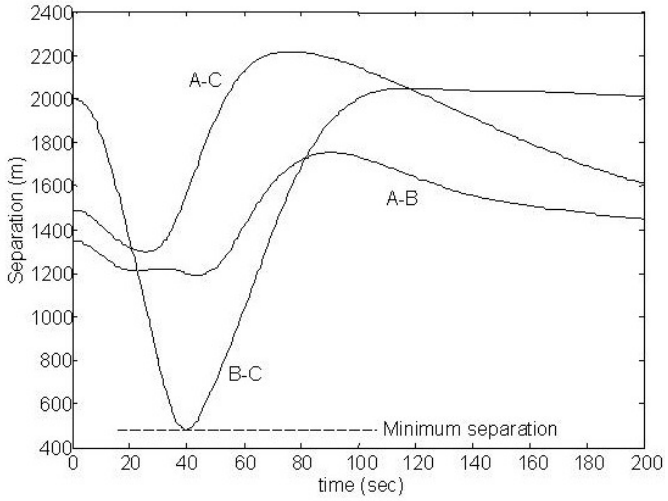

Figure 5(c). UAV formation separation time history.

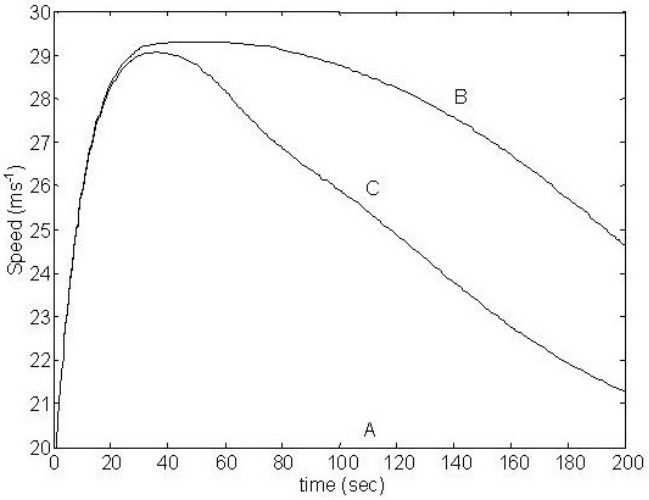

Figure 5(d). UAV formation speed time history.

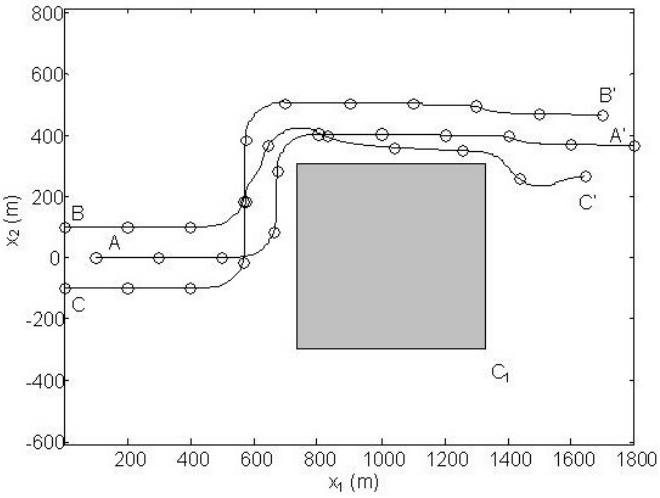

Figure 6. UAV formation manoeuvre at a single obstacle (o – 10s time steps).

with the remaining UAVs represented as mobile type II velocity fields. If required, the set of vectors $\Delta_i = (\Delta_{1i}, \Delta_{2i})$ can be rotated by the heading angle of the lead UAV to ensure that the formation rotates as a rigid body when the lead UAV turns. The speed of each member of the UAV formation can also be referenced to the lead UAV to ensure that the relative speed between the lead UAV and other UAVs in the formation will converge. For example, the following function for the speed of the ith ($i = 1 - (N - 1)$) UAV allows the UAVs to converge on the lead UAV while enforcing speed constraints

$$\delta_i = \delta_L \left(1 + \eta\left(1 - \exp\left(-\zeta|\mathbf{r}_i - \mathbf{r}_L|\right)\right)\right) \quad \ldots (27a)$$

$$\eta = \left(\frac{\delta_{\max}}{\delta_L} - 1\right) \quad \ldots (27b)$$

where η is a parameter which shapes the rate of convergence of the UAV speed to the lead UAV and $\upsilon_{\max}$ is the maximum enforced UAV speed. With this definition $\upsilon_i > \upsilon_L$ ($i = 1 - (N - 1)$) so that a minimum speed is also enforced. Since it is assumed that the speed of the lead UAV will never fall below stall speed, the stall speed constraint is then enforced through the entire formation.

An example of a re-formation manoeuvre with three UAVs is shown in Fig. 5(a). Here the lead UAV (*A*) maintains a constant heading and speed of 20ms^{-1} while *B* and *C* swap places in the formation. Due to the symmetry of this manoeuvre a collision between *B* and *C* would normally result. However, the UAVs turn to avoid each other, as shown in Fig. 5(b). The type II velocity fields associated with each UAV have been shaped using Equation (7) to enforce a minimum separation of 500m, as shown in Fig. 5(c). The speed of each UAV is also scaled using Equation (27) relative to the lead UAV speed of 20ms^{-1} and a maximum speed which has been defined as 30ms^{-1}, as shown in Fig. 5(d). A final example is shown in Fig. 6 where a triangular UAV formation negotiates an obstacle represented using a superquadratic generating function. Here it can be seen that as the lead UAV (*A*) manoeuvres to avoid the obstacle, *B* is displaced since it is referenced to *A* and so does not encounter

the obstacle. However, *C* does encounter the obstacle and falls in behind the lead UAV until the obstacle is successfully negotiated and the triangular formation can re-form.

7.0 CONCLUSIONS

A velocity field approach to UAV path-planning has been presented which allows single or multiple UAVs to manoeuvre between a start point *S* and goal point *G* without collision with static obstacles or other UAVs in a formation. Unlike heuristic path-planning algorithms, the velocity field algorithm presented here is based on mathematical rigour in that the properties of the Laplace equation can be invoked to demonstrate that the field will generate a unique path which is guaranteed to reach the goal *G*. In addition, since the velocity field can be generated analytically, the computational overhead to implement the algorithm is minimal, allowing autonomous operations with on-board path-planning.

ACKNOWLEDGMENTS

The work presented in this paper was undertaken with support from the Leverhulme Trust, to whom the author expresses his thanks.

REFERENCES

1. KHATIB, O. Real-time obstacle avoidance for manipulators and mobile robots, *Int J of Robotics Research*, **5**, (1), 1986, pp 90-98.
2. RIMON, E. and KODITSCHEK, D. Exact robot navigation using artificial potential functions, 1992, IEEE transactions on robotics and automation, **8**, (5), pp 501-518.
3. SATO, K. Dead-lock motion path planning using the Laplace potential field, *Advances in Robotics*, 1993, **17**, (5), pp 449-461.
4. GULDNER, J. and UTKIN, V. Sliding mode control for gradient tracking and robot navigation using artificial potential fields, 1995, IEEE Transactions on Robotics and Automation, **11**, (2), pp 247-254.
5. DE MEDIO, C., NICOLO, F. and G. ORIOLO. Robot motion planning using vortex fields, *Progress in Systems and Control Theory*, 1991, **7**, pp 237-244.
6. MASOUD, A. and BAYOUMI, M. Robot navigation using the vector potential approach, 1050-4729/93, 1993, Proceedings of the IEE international conference on robotics and automation, April 1993, Minneapolis.
7. SINGH, L., STEPHANOU, H. and WEN, J. Real-time robot motion control with circulatory fields, 1996, Proceedings of the IEE international conference on robotics and automation, April 1996, Minneapolis.
8. MASOUD, A. Using hybrid vector-harmonic potential fields for multi-robot, multi-target navigation in a stationary field, 1996, Proceedings of the IEE international conference on robotics and automation, April 1996, Minneapolis.
9. ZEGHAL, K. A Review of different approaches based on force fields for airborne conflict resolution, 1998, AIAA Guidance, navigation and control conference, August 1998, Boston.
10. SHAPIRA, I. and BEN-ASHER, J. Near-optimal horizontal trajectories for autonomous air vehicles, *J Guidance, Control and Dynamics*, 1997, **20**, (4), pp 735-741.
11. MCINNES, C. Potential function methods for autonomous spacecraft guidance and control, 1995, AAS 95-447, AAS/AIAA astrodynamics specialist conference, August 1995, Halifax, Nova Scotia.
12. GHOSH, R. and TOMLIN, C. Maneuver design for multiple aircraft conflict resolution, 2000, Proceedings of the American control conference, June 2000, Chicago.
13. VOLPE, R. and KHOSLA, P. Manipulator control with superquadratic artificial potential functions: theory and experiments, 1990, IEEE transactions on systems, man and cybernetics, **20**, (6), pp 1423-1436.
14. LORRAIN, P. and CARSON, D. *Electromagnetic Fields and Waves*, 1970, pp 303-308, Freeman, New York.
15. ARFKEN, G. *Mathematical Methods for Physicists*, 1985, pp 78-83, Academic Press, San Diego.
16. PACHTER, M., D'AZZO, J. and DARGAN, J. Automatic formation flight control, *J Guidance, Control and Dynamics*, 1994, **17**, (6), pp 1380-1383.
17. WOLFE, J., CHICHKA, D. and SPEYER, J. Decentralized controllers for unmanned aerial vehicle formation flight, 1996, Proceedings of the AIAA guidance, navigation and control conference, August 1996, San Diego.
18. RICHARDS, A., BELLINGHAM, J., TILLERSON, M. and HOW, J. Coordination of multiple UAVs, 2002, AIAA-2002-4588, AIAA guidance, navigation and control conference, August 2002, Monterey.